Eur. Phys. J. A **25**, 5–21 (2005)
DOI 10.1140/epja/i2004-10236-0

THE EUROPEAN PHYSICAL JOURNAL A

Low-spin states of doubly odd ^{184}Au

J. Sauvage[1,a], F. Ibrahim[1,2], B. Roussière[1], J. Genevey[2,b], A. Gizon[2], G. Marguier[3], P. Kilcher[1], A. Knipper[4], R. Béraud[3], G. Căta-Danil[2,c], F. Le Blanc[1], J. Obert[1], J. Oms[1], J.C. Putaux[1], C. Richard-Serre[4,6], A. Wojtasiewicz[1,5], and the ISOLDE and NICOLE Collaborations[6]

[1] Institut de Physique Nucléaire, IN2P3-CNRS/Université Paris-Sud, F-91406 Orsay Cedex, France
[2] Laboratoire de Physique Subatomique et de Cosmologie, IN2P3-CNRS/Université Joseph Fourier, F-38026 Grenoble Cedex, France
[3] Institut de Physique Nucléaire, IN2P3-CNRS/Université Claude Bernard, F-69621 Villeurbanne Cedex, France
[4] Institut de Recherches Subatomiques, IN2P3-CNRS, F-67037 Strasbourg, France
[5] Institute of Experimental Physics, Warsaw University, ul. Hoża 69, PL-00-681 Warsaw, Poland
[6] CERN, 1211 Genève 23, Switzerland

Received: 5 November 2004 / Revised version: 31 March 2005 /
Published online: 22 June 2005 –
Communicated by J. Äystö

Abstract. Low-spin states of ^{184}Au have been studied using the β^+/EC decay of ^{184}Hg. γ-ray and conversion-electron singles spectra were recorded with ^{184}Hg mass-separated sources. For γ-γ-t and X-γ-t coincidence measurements, mercury nuclei were produced in the ^{148}Sm + ^{40}Ar reaction and transported by a He-jet system. The electron spectra were recorded from ^{184}Hg sources produced at ISOLDE. A level scheme of ^{184}Au including 48 transitions is proposed. The experimental results are interpreted in the frame of a semi-microscopic axial-rotor–plus–two-quasiparticle model developed in the context of the HF+BCS approximation.

PACS. 21.10.-k Properties of nuclei; nuclear energy levels – 23.20.Nx Internal conversion and extranuclear effects – 23.20.Lv γ transitions and level energies – 27.70.+q $150 \leq A \leq 189$

1 Introduction

The neutron-deficient nuclei of the Pt, Au and Hg region are well known to exhibit low-energy shape coexistence [1]. The odd-odd nucleus ^{184}Au is located on the prolate edge of this region of shape instability. In this nucleus, the discovery by the NICOLE group at ISOLDE of a long-lived isomer linked to the ground state by an $M3$ isomeric transition caused a revival of interest [2]. From our partial level scheme established in the β^+/EC decay of ^{184}Hg to ^{184}Au, spin and parity values $I^\pi = 5^+$ and $I^\pi = 2^+$ have been assigned to the ground state and to the long-lived isomeric state, respectively [3]. From in-beam γ spectroscopy experiments new excited states and rotational-band structures have also been observed, but most of them could not be linked to the levels previously established in ^{184}Au [4].

More recently, resonance ionization spectroscopy was performed on desorbed Au atoms [5]. The complete hyperfine spectrum of both the $I^\pi = 2^+$ isomeric and the $I^\pi = 5^+$ ground states of ^{184}Au was recorded. The nuclear moments of both states and the mean square charge

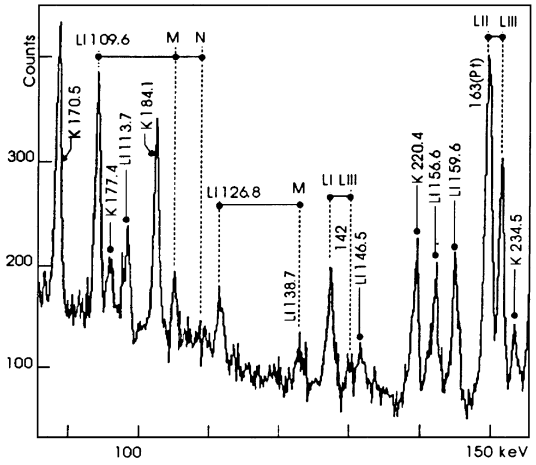

Fig. 1. Partial conversion-electron spectrum observed during the first experiment.

[a] e-mail: sauvage@ipno.in2p3.fr
[b] e-mail: genevey@lpsc.in2p3.fr
[c] *Permanent address*: Physics Department, Universitatea Politechnica, Bucarest, Romania.

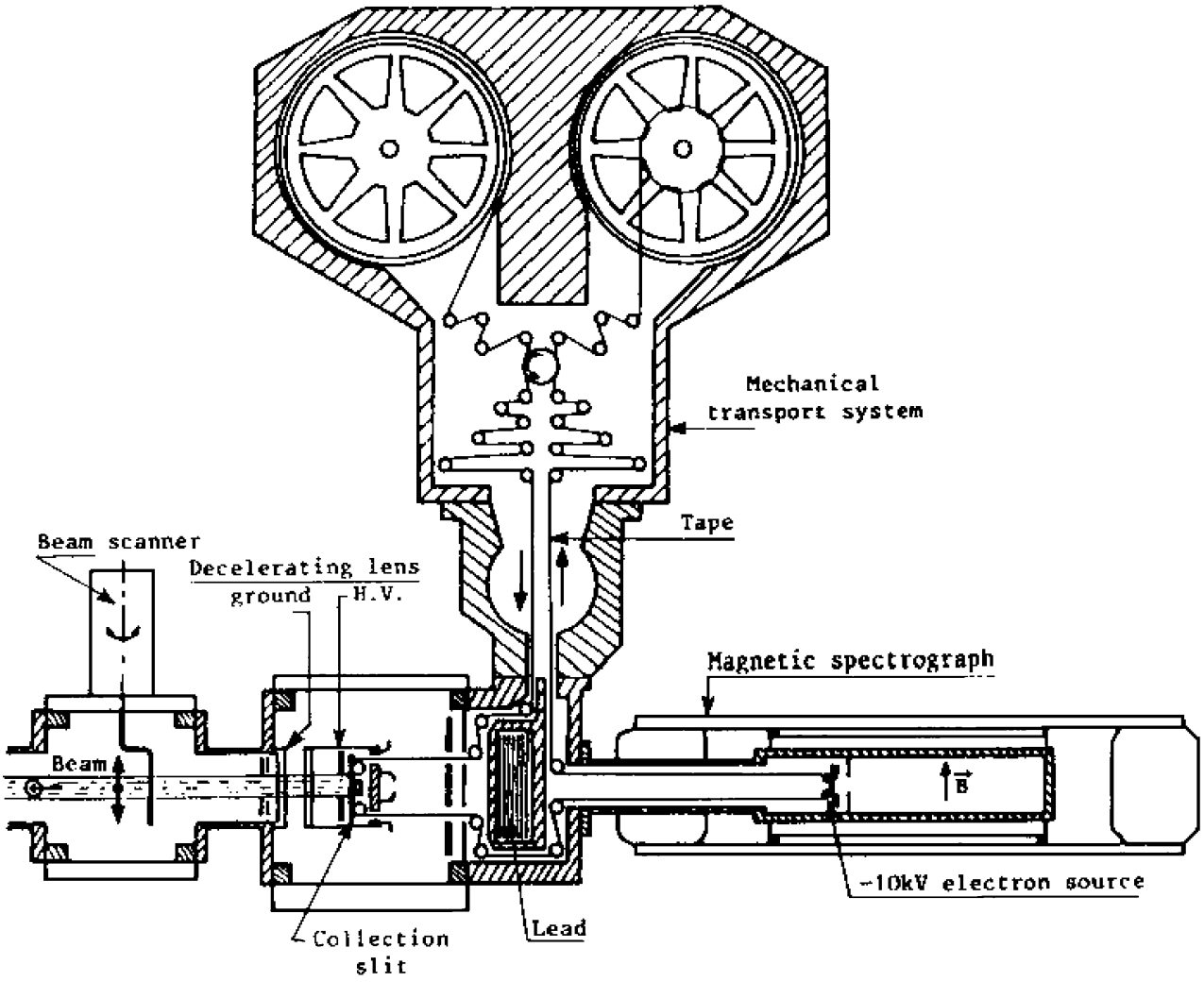

Fig. 2. High-resolution conversion-electron setup used at ISOLDE.

radius changes were extracted from the measurements. Thus, the structure of the 2^+ isomeric and 5^+ ground states of ^{184}Au has been determined as a proton in the $3/2^-[532]$ orbital coupled to the neutron in the $1/2^-[521]$ and $7/2^-[514]$ states, respectively. Furthermore, the nuclear deformations of these two states have also been determined; they are slightly different.

In this paper we report in more detail on the three series of experiments that we have performed to study the low-lying states of ^{184}Au populated in the β^+/EC decay of ^{184}Hg ($T_{1/2}$ = 30.6 s). The techniques employed are described in sect. 2. The experimental results as well as a level scheme of ^{184}Au with 19 excited states, previously reported as private communication in Nuclear Data Sheets [6] are presented and discussed in sect. 3. After that, the proposed level scheme is interpreted using the semi-microscopic axial-rotor–plus–two-quasiparticle model developed in the context of the Hartree-Fock–plus–BCS approximation [7].

2 Experimental procedures

2.1 Gamma-ray and conversion-electron measurements

2.1.1 First observation of conversion electrons in ^{184}Au

The first experiment has been performed at the ISOLDE facility at CERN in collaboration with the NICOLE group. Mercury atoms were produced by bombarding a molten-lead target by the SC 600 MeV proton beam. The obtained mass-separated ^{184}Hg beam was guided towards a counting station equipped of a Ge(Li) detector for γ-rays and a Si(Li) detector for electrons. Several cycles of collecting and counting times have been used to identify the various components involved in the ^{184}Hg, $^{184m+g}$Au, ^{184}Pt decay chain.

The first evidence of a strong 68.8 keV isomeric $M3$ transition is based on the observation of $L_{\rm I}$ (+ weak $L_{\rm II}$) and $L_{\rm III}$ electron lines detected with a Si(Li) detector. The result was already reported in ref. [2]. During the same run, data on both electrons and γ-rays in the range

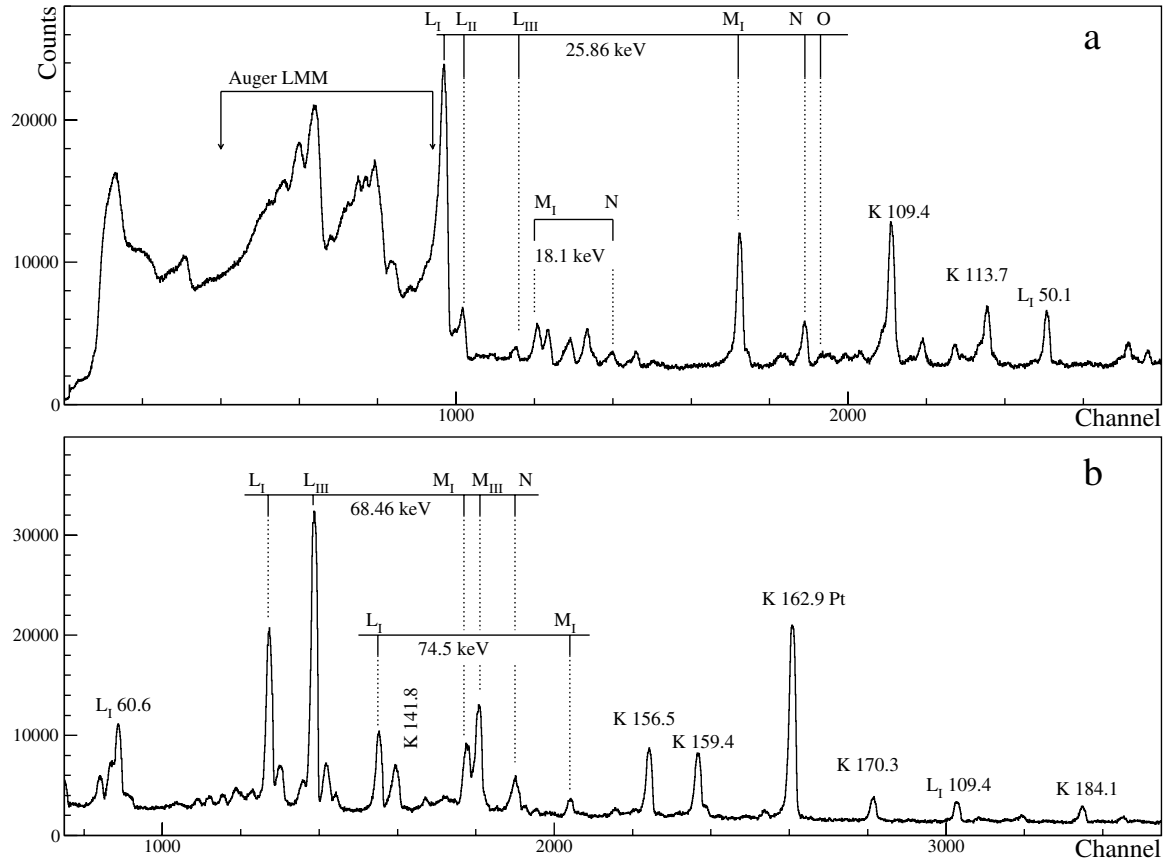

Fig. 3. Examples of two partial electron spectra measured with the spectrograph + film system.

20–500 keV were obtained for a 6 s collecting time —12 s counting time cycle. A partial ^{184}Au electron spectrum recorded with the Si(Li) detector is shown in fig. 1. Intensities of γ-rays reported in table 1 have been obtained in this measurement with the Ge(Li) detector calibrated in energy and efficiency at the counting station. The energies and K, L conversion coefficients given in table 1 for the transitions with an energy larger than 200 keV have been obtained in this experiment.

2.1.2 The high-resolution conversion-electron measurement

An additional high-resolution conversion-electron measurement has been undertaken to obtain more precise electron energies and intensities and to attribute unambiguously the multipolarities to a large number of transitions. In this experiment, states in ^{184}Au were populated through the β^+/EC decay of ^{184}Hg. Mercury atoms were produced at ISOLDE (CERN) by bombarding a molten-lead target by the PS-Booster 1 GeV proton beam. The radioactive ions extracted from the ion source were then mass-separated and guided through a beam line to the experimental setup devoted to the detection of low-energy conversion electrons with high energy resolution. This apparatus consists of a 180° magnetic spectrograph associated with a tape transport system (see fig. 2). The 60 keV incoming ions are decelerated down to 700 V before being collected on the tape, in order to prevent a deep implantation. The collected radioactive source is transported into the spectrograph and then about −10 kV high voltage is applied to the source in order to accelerate the emitted electrons. These accelerated electrons, entering the magnetic field, are deviated in order to reach a photographic film (Kodak, DEF392) used as a detector. The magnetic induction (B) and the preacceleration high voltage (HV) applied define the energy range of the conversion electrons detected. With $B = 60.7 \cdot 10^{-4}$ T and $HV = -12.6$ kV, a conversion-electron energy range (1.5–110 keV) is covered. It is important to determine precisely the values of the magnetic induction and of the preacceleration high voltage as well as the response of the system as a function of the impact energy of the electrons. These determinations have been made using the ^{187}Au → ^{187}Pt [8] and the ^{187}Pt → ^{187}Ir [9] decays for which electron transition energies and intensities are well known, in the 10 to 100 keV energy range.

More details on the experimental setup can be found elsewhere [10–12].

Two partial electron spectra obtained with ^{184}Hg separated samples are shown in fig. 3. The high quality of the data is specially illustrated by the electron lines belonging to the 25.86 keV and 68.46 keV transitions in ^{184}Au. The internal-conversion coefficients calculated using the relative-efficiency curve shown in fig. 4 are reported in table 1, column 3. Obviously, for the very low-energy

Table 1. γ-ray and internal-conversion electron data for the ^{184}Hg $\rightarrow$ ^{184}Au decay.

E_γ (keV)	I_γ	$ICC_{\rm exp}$ or ratios or comments	Multipolarity
3.4 (2)		$N_{\rm I}$ and O lines observed	$(M1)$
18.1(2)	2.3(7)	$\alpha_{LI} = 130(25)$, $L_{\rm I}/L_{\rm II} = 1/0.11(1)$	$M1$
25.86(6)	19(2)	$\alpha_{LI} = 52(10)$, $\alpha_{L\rm II} = 6.3(10)$, $L_{\rm II}/L_{\rm III} = 1/0.36(10)$, $M_{\rm I} + M_{\rm II}/M_{\rm III} = 1/0.04(1)$	$M1 + 0.17(10)\%$ $E2$
29.4(1)	1.5(3)	$\alpha_{LI} = 38(18)$, $L_{\rm I}/L_{\rm II} = 1/0.4$, $\alpha_{MI} = 8.7(2)$	$M1+ \approx 2\%$ $E2$
30.3(1)	1.7(4)	$\alpha_{LI} = 35(10)$, $\alpha_{L\rm III} = 21(8)$	$M1+ \approx 4\%$ $E2$
42.7(1)	1.9(4)	$\alpha_{LI} \leq 22$, $\alpha_{L\rm III} < 1.8$	$M1(+E2)$
43.3(3)	4.3(6)	only weak mixed electron lines observed	–
45.8(1)	2.0(3)	$\alpha_{LI} = 13(3)$, $L_{\rm I}/L_{\rm III} \approx 1/0.12$	$M1+ \approx 1\%$ $E2$
47.6(2)	2.1(5)	$\alpha_{LI} = 8(2)$, $\alpha_{MI} = 1.9(10)$	$M1$
50.1(1)	7(1)	$\alpha_{LI} = 8.5(15)$, $L_{\rm I}/L_{\rm II} = 1/0.13(2)$	$M1(+E2)$
57.3(2)	4(2)	$\alpha_{L\rm II} \simeq \alpha_{L\rm III} = 12(6)$, $L_{\rm I}/L_{\rm II}/L_{\rm III} = 1/7.2(15)/6.9(15)$	$E2+ \approx 40\%$ $M1$
59.0(2)	5(1)	$L_{\rm I}$, $L_{\rm III}$ electron lines not observed	$E1$
60.6(1)	26(4)	$\alpha_{LI} = 4(1)$, $L_{\rm I}/L_{\rm II}/L_{\rm III} = 1/0.13(3)/< 0.04$, $\alpha_{MI} = 0.9(1)$	$M1$
68.46(4)	–	see text and table 3	$M3$
74.5(2)[d]	40(4)	$\alpha_{LI} = 2.4(4)$, $M_{\rm I}/M_{\rm II}/M_{\rm III} = 1/0.21/0.09$	$M1$+$E2$
81.9(1)	60(8)	$\alpha_{(LI+L\rm II)} \leq 0.3$	$E1$
92.0(1)	53(6)	$\alpha_{LI} \leq 0.1$, $\alpha_{L\rm III} \leq 0.05$	$E1$
104.6(2)	2.8(6)	$\alpha_K = 6.8(20)$, $\alpha_{LI} = 1.3(6)$,	$M1$
109.4(1)	15(3)	$\alpha_K = 14(4)$, $\alpha_{LI} = 2.3(5)$	$M1$+$E0$, abn. $M1$
110.8(2)	5(1)	$\alpha_K = 7(3)$	$(M1)$
112.6(2)	4(1)	$\alpha_K = 3.6(10)$	$(M1)$
113.7(1)	16(3)	$\alpha_K = 4.6(6)$, $\alpha_{LI} = 1.0(4)$	$M1$
126.7(1)	13(3)	$\alpha_K = 2.0(6)$, $\alpha_{(LI+L\rm II)} = 0.62(15)^{(*)}$, $\alpha_{L\rm III} \leq 0.15^{(*)}$	$M1(+E2)$
127.3(2)	27(4)	$\alpha_K \leq 0.4$, $\alpha_{L\rm III} \leq 0.1^{(*)}$	$E1$
138.5(2)	6(2)	$\alpha_K = 2.9(8)$	$M1$
141.8(1)[a]	32(4)	$\alpha_K = 1.8(5)$, $\alpha_{(LI+L\rm II)} = 0.45(9)^{(*)}$, $\alpha_{L\rm III} = 0.09(4)^{(*)}$	$E1+ \approx 13\%$ $M2$, $M1+ \approx 26\%$ $E2$
146.5(4)	24(8)	$\alpha_K \leq 3.5$, $\alpha_{(LI+L\rm II)} = 0.26(10)^{(*)}$, $\alpha_{L\rm III} \leq 0.08^{(*)}$	$M1(+E2)$
156.5(1)	1020(100)	$\alpha_K = 0.10(2)$, $\alpha_{(LI+L\rm II)} = 0.012(4)^{(*)}$	$E1$
159.4(1)	60(8))	$\alpha_K = 1.4(4)$, $\alpha_{(LI+L\rm II)} = 0.27(6)^{(*)}$	$M1$
160.0(1)	23(5)	$\alpha_K = 0.3(2)$	$E1$
170.3(1)	24(4)	$\alpha_K = 1.3(3)$	$M1$
177.3(2)	26(4)	$\alpha_K < 0.3$	$E1$,$E2$
178.1(2)	6(2)	$\alpha_K \leq 0.4$	$E1$,$E2$
181.3(2)	6(2)	$\alpha_K < 0.3$	$E1$,$E2$
182.5(2)	6(2)	$\alpha_K < 0.15$	$E1$
184.1(2)	3(1)	$\alpha_K = 6(2)^{(*)}$, $\alpha_{(LI+L\rm II)} = 1.7(8)^{(*)}$	$M2$
185.8(1)	12(2)	$\alpha_K < 0.17$	$(E1)$
220.4(1)	26(3)	$\alpha_K = 0.54(12)^{(*)}$, $\alpha_{(LI+L\rm II)} = 0.11(3)^{(*)}$	$M1$
234.5(3)	22(5)	$\alpha_K = 0.3(2)^{(*)}$, $\alpha_L < 0.1^{(*)}$	$(M1 + E2)$
236.7(1)	1000(100)	$\alpha_K = 0.04(1)^{(*)}$, $\alpha_L = 0.05(2)^{(*)}$	$E1$
238.4(2)	180(30)	$\alpha_K = 0.46(11)^{(*)}$, $\alpha_L = 0.08(2)^{(*)}$,$\alpha_M = 0.02(1)^{(*)}$	$M1$
244.8(2)	9(2)		–
248.0(2)	9(3)		–
259.5(1)	86(10)	$\alpha_K = 0.39(7)^{(*)}$, $\alpha_{(LI+L\rm II)} = 0.06(7)^{(*)}$	$M1$
262.9(1)	62(8)	$\alpha_K = 0.38(7)^{(*)}$, $\alpha_{(LI+L\rm II)} = 0.07(2)^{(*)}$	$M1$
277.7(2)	15(3)	$\alpha_K = 0.37(9)^{(*)}$, $\alpha_{(LI+L\rm II)} = 0.04(2)^{(*)}$	$M1$
291.5(2)	17(3)	$\alpha_K = 0.30(9)^{(*)}$, $\alpha_{(LI+L\rm II)} = 0.05(2)^{(*)}$	$M1$
294.8(3)	20(6)	$\alpha_K = 0.30(15)^{(*)}$	$(M1)$
295.7(1)	100(15)	$\alpha_K = 0.28(8)^{(*)}$, $\alpha_{(LI+L\rm II)} = 0.08(3)^{(*)}$	$M1$
313.1(2)	33(5)	$\alpha_K = 0.22(6)^{(*)}$, $\alpha_{(LI+L\rm II)} = 0.05(2)^{(*)}$	$M1$
331.5(2)	10(2)	$\alpha_K = 0.32(13)^{(*)}$	$(M1)$
348.2(2)	18(3)	$\alpha_K = 0.17(5)^{(*)}$, K/$L \approx 5.6$ $^{(*)}$	$M1$
362.0(2)	25(10)	$\alpha_K = 0.16(8)^{(*)}$	$(M1)$
372.2(2)	9(2)	–	–
404.7(2)	22(3)	–	–
419.6(4)	5(2)	–	–
422.7(2)	42(6)	–	–

([d]) Double line observed from γ-γ coincidences, see text; ([a]) $E1 + M2$ retained from γ-γ coincidences and level scheme; (*) Seen with the Si(Li) detector.

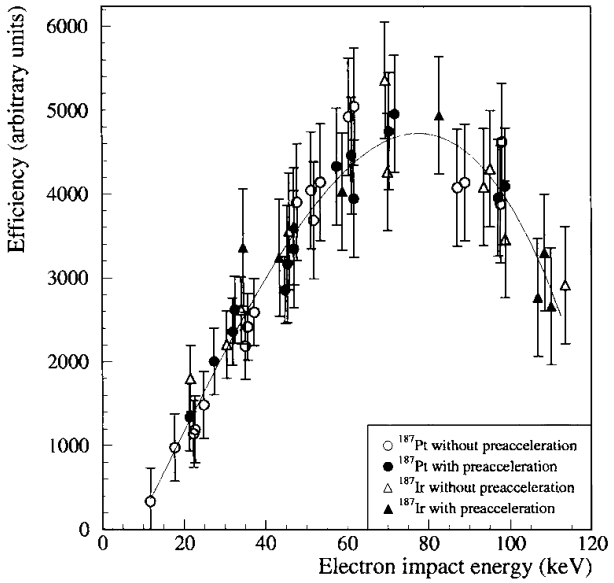

Fig. 4. Relative-efficiency calibration of the spectrograph + film system measured by using ^{187}Au and ^{187}Pt sources.

strongly converted transitions the ratios L_i/L_j or M_i/M_j have been used to deduce the multipolarities indicated in table 1, column 4.

2.2 γ-γ coincidence measurements

Low-spin excited states of ^{184}Au have been investigated from the β^+/EC decay of ^{184}Hg nuclei. The radioactive Hg isotopes were produced by bombarding a self-supporting 2 mg/cm^2 ^{148}Sm target with a 185 MeV energy ^{40}Ar^{11+} beam delivered by the SARA accelerator in Grenoble. A He-jet system was used to carry the produced radioactive atoms to a low-background counting room [13]. The ^{148}Sm target was placed in a reaction chamber in which the helium circulated. A 2 mg/cm^2 Havar window was used as a separation between the vacuum of the cyclotron and the reaction chamber with a helium pressure of about 1 kg/cm^2. In this "thermalization chamber" the reaction products were flown down to thermal velocities by collision with the buffer gas atoms. Together with the gas, the thermalized atoms were then sucked via a 12 m long and 1.2 mm diameter capillary in a low-pressure "collection chamber". As previously recommended [14], we added some iodine to the helium to extract mercury isotopes with a quite good efficiency. This is clearly illustrated in fig. 5. The reaction products were collected during 30 s and measurements were performed during 30 s. Singles γ-ray spectra were obtained with three detectors: a planar Ge X-ray detector with a resolution of 0.9 keV FWHM at 122 keV covering an energy range up to 1 MeV, and two Ge(HP) detectors, of respectively, 60% and 34% efficiencies and 2.3 and 2.2 keV FWHM resolution at 1.3 MeV, covering an energy range up to 1.3 MeV. A total of 56×10^6 X-γ-t and 31×10^6 γ-γ-t coincidence events were obtained during the 95 h experiment. Singles γ-spectra were analysed using the GAMANAM curve fitting code [15,16], a modified version of the GAMANAL code. The X-γ-t and γ-γ-t coincidence events obtained in the experiment were sorted to get prompt-, total- and delayed-coincidence bidimensional matrices.

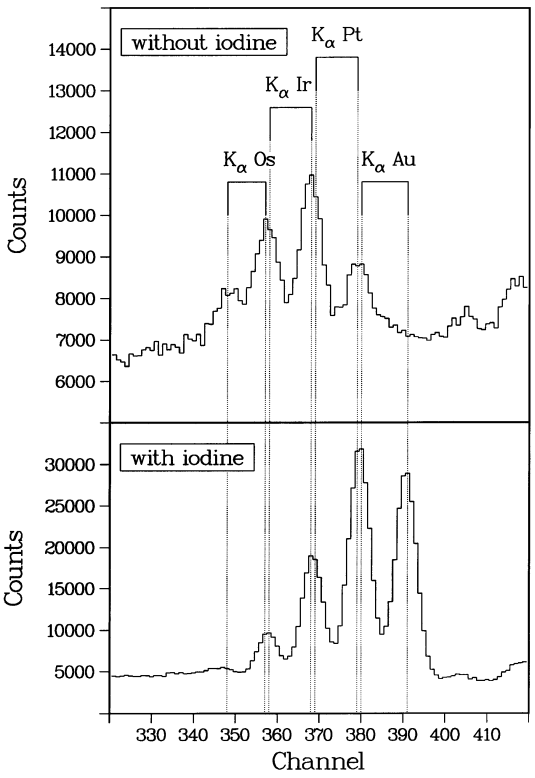

Fig. 5. Comparison of K_α X-rays detected in collected samples shows clearly the role of iodine added to He in the extraction of Hg isotopes. (Au K_α X-rays are associated to the ^{184}Hg $\rightarrow$ ^{184}Au decay.)

The prompt- and delayed-coincidence matrices were got using 60 and 100 ns time windows, respectively. In order to get coincidences with lines placed above or below the 69 ns isomer the delayed windows were placed before and after the prompt one.

These matrices were analysed using either SUN or MILFEUIL programs [17]. Examples of γ-γ prompt-, total- or delayed-coincidence spectra are shown in figs. 6 and 7 while the main coincident γ-rays are listed in table 2, column 3.

3 Results

3.1 Energy and multipolarity of the isomeric transition

Due to both the quality of the high-resolution electron spectrum observed (fig. 3b) and the precise internal energy calibration based on well-known lines belonging to the ^{187}Au $\rightarrow$ ^{187}Pt and the ^{187}Pt $\rightarrow$ ^{187}Ir decays, a very precise energy has been deduced for the ^{184}Au isomeric transition. The existence of this transition was reported for the first time by Eder *et al.* at 68.8 keV [2]. From the present

Table 2. γ-γ coincidences observed in the ^{184}Hg $\rightarrow$ ^{184}Au decay for the γ transitions placed in the ^{184}Au level scheme.

E_γ (keV)	I_γ	Main coincidences observed	Location in the scheme
18.1(2)	2.3(7)	–	(86.6 → 68.5)
25.9(1)	19(2)	156.5-236.7	254.3 → 228.4
42.7(1)	1.9(4)	–	(129.2 → 86.6)
47.6(1)	2.1(2)	(25.9)	(301.9 → 254.3)
50.1(1)	7(1)	(244.8)-259.5-262.9	381.5 → 331.4
57.3(1)	3(2)	(113.7)	129.2 → 71.9
59.0(1)	5(1)	–	(301.9 → 242.9)
60.6(1)	26(4)	113.7-348.2-362.0	129.2 → 68.5
74.5(2)	33(4)[a]	(109.4)-220.4-238.4	381.5 → 306.9
74.5(2)	7(4)[a]	81.9	146.5 → 71.9
81.9(1)	60(8)	74.5-92.0-127.3-146.5-170.3-236.7	228.4 → 146.5
92.0(1)	53(6)	81.9-156.5-170.3	320.4 → 228.4
104.6(2)	2.8(6)	(74.5)-(220.4)-238.4-(259.5)-(262.9)	486.1 → 381.5
109.4(1)	15(3)	(74.5)-(127.3)-238.4-294.8	491.0 → 381.5
113.7(1)	16(3)	(57.3)-60.6	242.9 → 129.2
126.7(1)	13(3)	277.7-295.7	491.0 → 364.2
127.3(2)	27(4)	(25.9)-(109.4)-156.5	381.5 → 254.3
138.5(2)	6(1)	–	(381.5 → 242.9)
141.8(1)	32(4)	236.7	228.4 → 86.6
146.5(4)	24(8)	81.9-(92.0)-(236.7)	146.5 → 0.0
156.5(1)	1020(100)	25.9-(57.3)[b]-92.0-127.3-(146.5)[b]- 170.3-181.3-236.7-372.2	228.4 → 71.9
159.4(1)	60(8)	244.8-259.5-262.9	491.0 → 331.4
160.0(1)	23(5)	236.7	228.4 → 68.5
170.3(1)	24(4)	92.0-156.5-(331.4)[b]	491.0 → 320.4
181.3(2)	6(2)	156.5	409.7 → 228.4
182.5(2)	6(2)	236.7	254.3 → 71.9
184.1(2)	3(1)	–	(486.2 → 301.9)
185.8(1)	12(2)	236.7	254.3 → 68.5
220.4(1)	26(3)	74.5	306.9 → 86.6
234.5(3)	22(5)	60.6-113.7	477.4 → 242.9
236.7(1)	1000(100)	25.9-81.9-(112.6)[b]-141.8-(146.5)-156.5-160.0-182.5-185.8	491.0 → 254.3
238.4(2)	180(30)	74.5	306.9 → 68.5
244.8(2)	9(2)	(50.1)-(159.4)	331.4 → 86.6
248.0(2)	9(3)	–	(491.0 → 242.9)
259.5(1)	86(10)	50.1-159.4	331.4 → 71.9
262.9(1)	62(8)	50.1-159.4	331.4 → 68.5
277.7(2)	15(3)	(126.7)	364.2 → 86.6
294.8(3)	20(6)	–	381.5 → 86.6
295.7(1)	100(15)	126.7	364.2 → 68.5
313.1(2)	33(5)	–	(381.5 → 68.5)
348.2(2)	18(3)	60.6	477.4 → 129.2
362.0(2)	25(10)	(57.3)-60.6	491.0 → 129.2
372.2(2)	9(2)	156.5	600.6 → 228.4
404.7(2)	22(3)	–	491.0 → 86.6
419.6(4)	5(2)	–	491.0 → 71.9
422.7(2)	42(6)	–	491.0 → 68.5

([a]) Deduced from the γ-γ coincidences and the total intensity of the doublet.
([b]) Coincidences probably due to background since no confirmation could be found. However, we reported them in the table even though they contradict the level scheme because they could be hints of the existence of doublets.

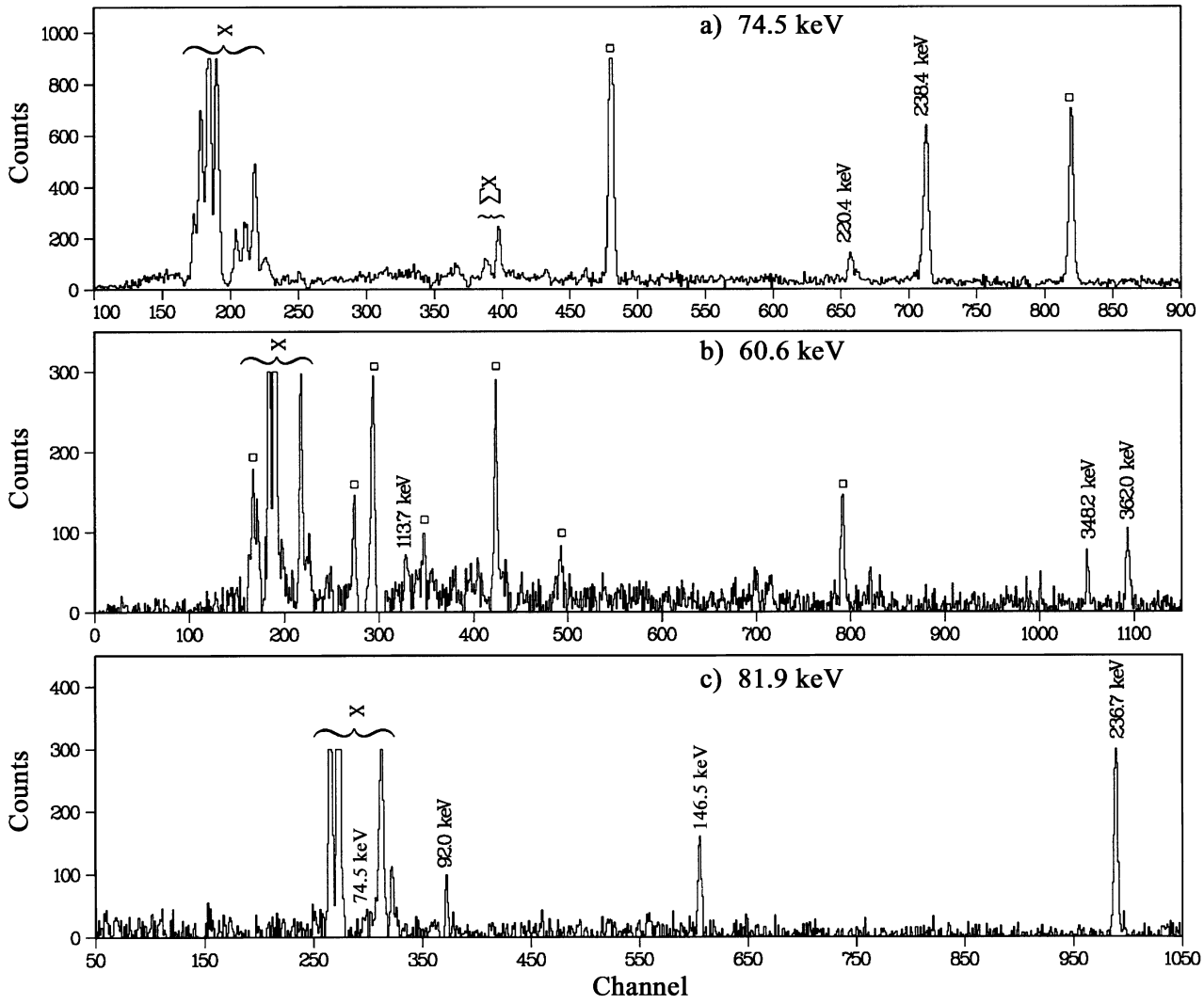

Fig. 6. Prompt γ-γ coincidence spectra gated by the transitions at 74.5, 60.6, 81.9 keV, respectively. The γ lines marked by an open square are due to the decay of the Havar window reaction products.

measurement, the energy deduced from the average of the $L_{\rm I}$, $L_{\rm II}$, $L_{\rm III}$, $M_{\rm I}$, $M_{\rm II}$, $M_{\rm III}$, $N_{\rm I}$ and $N_{\rm III}$ line energies is estimated to be 68.46(4) keV. From the experimental ratios of the intensities of the electron lines, an $M3$ multipolarity is confirmed (see table 3). The errors on the electron line intensities reported in table 3 include the statistic errors on the electron lines and on the subtracted contributions induced by other conversion-electron and Auger lines. The experimental ratios $(L_{\rm I}+L_{\rm II})/L_{\rm III}/\Sigma M/\Sigma N/\Sigma O =$ 1/1.7(3)/0.88(13)/0.19(6)/0.078(37) are in very good agreement with the theoretical ones 1/1.92/0.88/0.248/ 0.046 expected for a 68.46 keV $M3$ transition in gold. The energies listed in table 1, column 1, for most of the other low-energy transitions ($E < 180$ keV) have also been deduced from the conversion-electron spectrum.

3.2 Multipolarity of transitions in ^{184}Au

For the determination of the experimental conversion coefficients, the electron intensities have been normalized using the $E2$, 162.9 keV transition present in the ^{184}Au $\rightarrow$ ^{184}Pt decay. The experimental conversion coefficients obtained in this work are listed in column 3 of table 1.

Table 3. Data on conversion-electron lines of the 68.46 keV $M3$ isomeric transition in ^{184}Au.

e$^-$ line	I (ΔI)	ICC ($M3$)
$L_{\rm I}+L_{\rm II}$	232(35)	789[a]
$L_{\rm III}$	397(60)	1515[a]
ΣM	197(30)	696[a]
ΣN	45(7)	196[b]
ΣO	18(6)	36[b]

([a]) Reference [18].
([b]) Reference [19].

Most of the coefficients have been determined using the precise intensities obtained with the high-resolution spectrograph, whereas data on electrons with energies larger

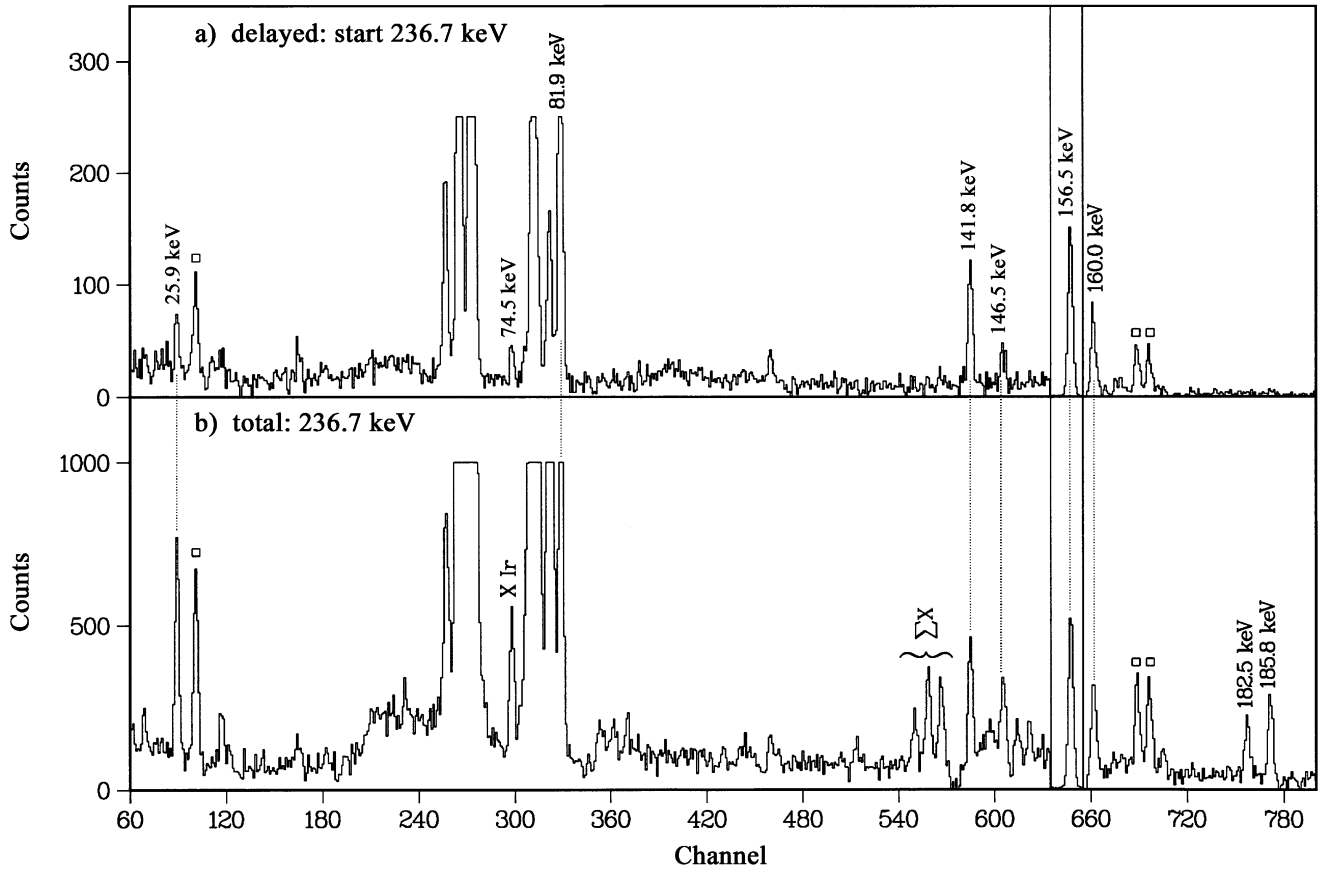

Fig. 7. γ-γ coincidences with the 236.7 keV transition: the spectrum labelled b) corresponds to the total time gate, while the delayed spectrum labelled a) is gated by the "start 236.7 keV" line. The γ lines marked by an open square are due to the decay of the Havar window reaction products. The gamma intensity of the 156.5 keV transition has been divided by a factor of ten.

than 106 keV were obtained in the experiment at ISOLDE by using the Si(Li) detector. The most probable multipolarities, deduced from the comparison of the experimental conversion coefficients to the theoretical ones [18,19] are indicated in column 4 of table 1. Large uncertainties exist for absolute conversion coefficients of the very low-energy strongly converted transitions. In such cases, the multipolarities are essentially based on L_i/L_j and/or M_i/M_j ratios. For a few transitions observed in the present work, the following comments are needed:

i) The doublet indicated at 74.5 keV in table 1 cannot be resolved in the singles gamma spectra. The separation in two components is observed in the γ-γ coincidence spectra. It supports the $M1+ E2$ mixing indicated in table 1, column 4.
ii) The large internal conversion of the 109.4 keV transition is clearly seen in fig. 3a by comparing the intensities of the $K_{109.4}$ and $K_{113.7}$ conversion lines, while $I_\gamma(109.4) = I_\gamma(113.7)$. These results support the $(M1{+}E0)$ or abnormal $M1$ [20] multipolarity listed for the 109.4 keV transition in table 1.

3.3 Level scheme of ^{184}Au

The level scheme of ^{184}Au shown in fig. 8 has been built using energies, intensities and multipolarities of the γ lines listed in table 1 and the coincidence data reported in table 2. The identification of the transitions belonging to the ^{184}Hg $\rightarrow$ ^{184}Au decay has been obtained by analysing the spectrum in coincidence with the only pure X-ray of gold, namely the 68.8 keV K_{α_1}.

Three of these transitions (25.9, 156.5 and 236.7 keV) have a total intensity 10 times greater than the others and are in coincidence with each other. In fig. 7 we present the γ-spectra in coincidence with the 236.7 keV transition for the delayed and total matrices, respectively. It clearly appears that the 25.9 keV is in prompt coincidence with the 236.7 keV transition, while the 156.5 keV transition is stronger in delayed coincidences. In fig. 7b two transitions (182.5 and 185.8 keV) appear with the same intensity ratio as that in the singles γ-spectrum. The difference in energy between these two transitions is close to the one between the two others at 156.5 and 160.0 keV transitions. Moreover, the differences in energy between the 182.5 keV and the 156.5 keV transitions and between the 185.8 keV and the 160.0 keV transitions are, respectively, equal to 26.0 and 25.8 keV. This allows us to propose the position of the 25.9 keV transition in the 156.5-25.9-236.7 keV cascade and the existence of an isomeric level at 228.4 keV (fig. 8).

To determine the half-life of the 228.4 keV level, we have studied the time spectrum of the 236.7-156.5 keV

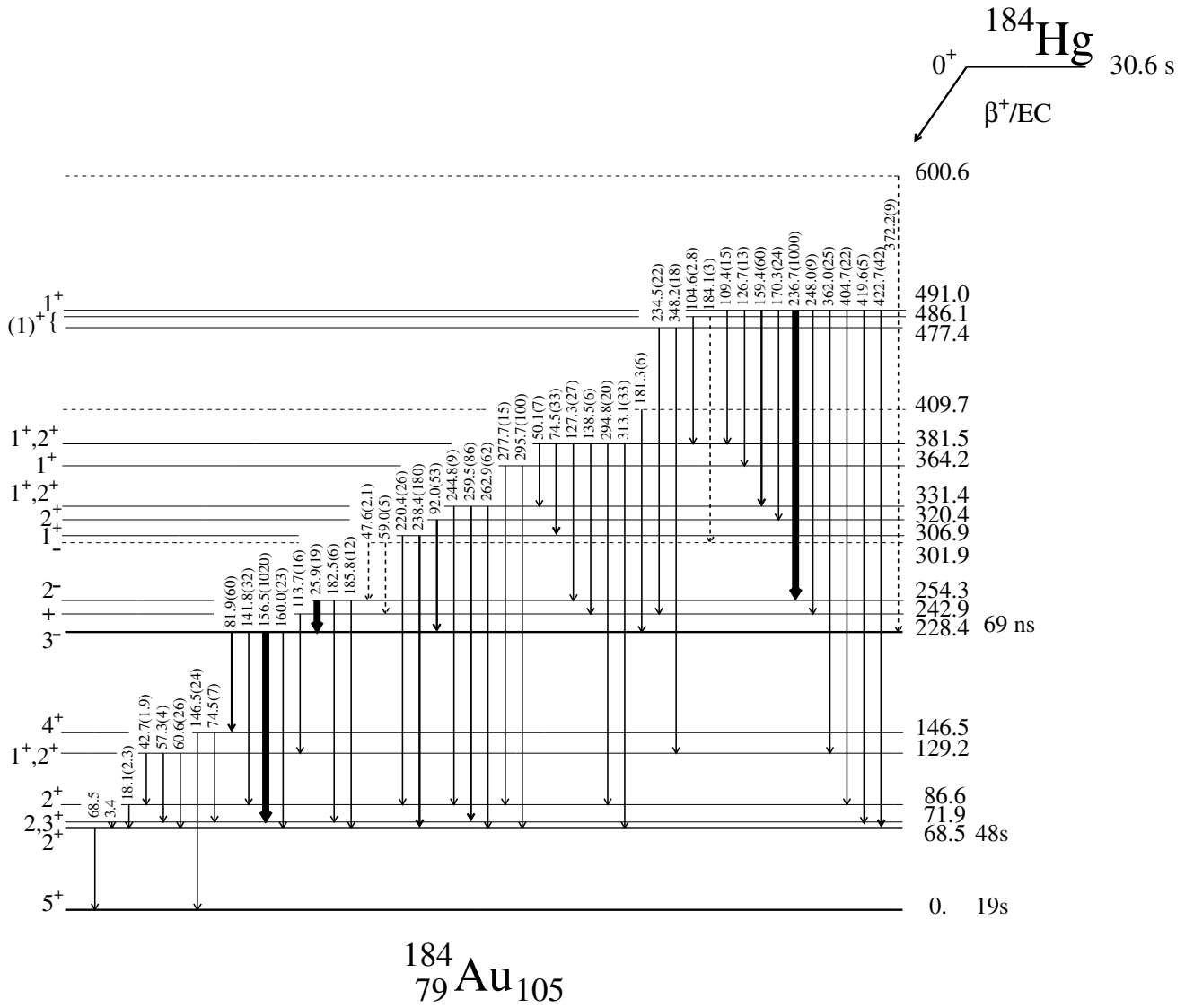

Fig. 8. Low-spin state level scheme of ^{184}Au. The isomer and ground-state half-lives have been estimated to be $T_{1/2,\mathrm{m}} = 48$ s and $T_{1/2,\mathrm{g}} = 19$ s or 21 s from [21,22]. Energies of transitions and levels are in keV. Gamma intensities are given in round brackets.

cascade. The result of this investigation has already been presented in [3]; the half-life of the 228.4 keV level is equal to $T_{1/2}(228.4\,\mathrm{keV}) = 69 \pm 6$ ns.

The existence of this isomeric state has been decisive to build the level scheme. Indeed, from the analysis of the delayed γ-γ coincidences, one can select the γ transitions placed above or below the isomer. In particular, the lines at 60.6, 74.5, 81.9, 141.8, 146.5 and 160.0 keV, similarly to the strong 156.5 keV, are below the isomeric state. The 146.5 keV transition which is in prompt coincidence with the 81.9 keV (fig. 6c) appears to be the only one that feeds directly the ground state as a "by-pass" of the isomeric state at 68.5 keV.

In the level scheme of ^{184}Au displayed in fig. 8, some transitions have been placed because their energies correspond to a difference between two levels firmly established by γ-γ coincidences. This is the case for the 404.7, 419.6 and 422.7 keV transitions feeding, respectively, the 86.6, 71.9 and 68.5 keV levels.

A few excited states are only tentative with no parity assignment, as those at 409.7 keV or 600.6 keV. The one at 301.9 keV decaying via two transitions at 47.6 keV ($M1$) and 59.0 keV ($E1$) which are too weak to be seen in γ-γ coincidences, has probably a negative parity.

It is worth noting that a possible $E0$ part in the 109.4 keV could help to limit the spin values of some states but the high conversion coefficient of this transition can be also due to an abnormal $M1$ multipolarity [23,24, 20]. Our data, unfortunately, do not allow us to distinguish between these two possibilities. In the present work about 96% of the total intensity has been placed in the level scheme. Table 4 presents the β^+/EC feedings for all the ^{184}Au excited levels. For some levels the β^+/EC feedings can be equal to 0 within the error bars, in this

Table 4. (β^+/EC) feedings of ^{184}Au levels and logft values for selected transitions of the ^{184}Hg decay.

Level energy (keV)	$I(\beta^+/\mathrm{EC})$ (%)	logf_0t
86.6	6.4±6.5	
129.2	6.7±5.5	$5.3^{+0.8}_{-0.3}$
146.5	0.5±2.1	
228.4	−3.9±13.0	
242.9	1.0±1.2	
254.3	11.4 ±11.4	
301.9	0.3 ±0.4	
306.9	6.8± 2.6	$5.3^{+0.2}_{-0.1}$
320.4	0.6± 0.7	
331.4	−0.8± 2.3	
364.2	3.7±1.3	$5.5^{+0.2}_{-0.1}$
381.5	2.1±3.9	
409.7	0.3±0.1	$6.6^{+0.2}_{-0.1}$
477.4	1.9±0.4	5.8±0.1
486.1	1.6±0.4	$5.8^{+0.2}_{-0.1}$
491.0	61.0±8.2	4.2±0.1
600.6	0.3±0.1	6.5±0.1

case the logft values have not been calculated. For the other levels the logft values have been calculated using $Q_{\mathrm{EC}} = 3.76$ MeV. This value was obtained in the following way. From the measurement previously reported on the ^{184}Au level scheme [25], Dautet *et al.* [26] determined a $Q_{\mathrm{EC}} = 3.66(3)$ MeV for the ^{184}Hg decay. From the new level scheme established in this work, the level with the strongest β^+ feeding is located at 491.0 keV instead of 392 keV, which leads to $Q_{\mathrm{EC}} = 3.76(3)$ MeV. The Q_{EC} value used in the present work is different from the value reported in ref. [27], $Q_{\mathrm{EC}} = 3.97$ MeV. However, the logft values deduced are very similar: log $ft = 4.3$ (1) instead of 4.2 (1) for the 491.0 keV level.

It is known that logft values lower than 5.9 correspond to allowed transitions $\Delta J = 0, 1$ with $\Delta\Pi = +$, except $0^+ \rightarrow 0^+$ [28]. The 491.0 keV excited state receives about 60% of the intensity and is associated to a logft value of 4.2(1). Since the ^{184}Hg ground state has 0^+ as spin and parity, the 491.0 keV excited state in ^{184}Au has unambiguously spin and parity $I^\pi = 1^+$. Except for this level most of the feedings reach only a few percent but, in some cases, the maximum logft values (see table 4) are found to be lower than 5.9. This indicates that the most probable spin and parity values of the 306.9 and 364.2 levels are 1^+. It can be noted that the total disintegration percentage collected by the levels appearing to be fed from table 4 is equal to 82.3%, the missing percentage can be due to the unplaced transitions. Indeed they represent only 4% of the total intensity, but could correspond up to 18.5% of the disintegrations.

Therefore, spin and parity of levels indicated in fig. 8 are based on I^π(g.s.) = 5^+, I^π(68.5 keV isomer) = 2^+, $I^\pi(491.0\,\mathrm{keV}) = 1^+$, $I^\pi(364.2\,\mathrm{keV}) = 1^+$, $I^\pi(306.9\,\mathrm{keV}) = 1^+$, and the multipolarities of the transitions reported in table 1. As an example, the level at 320.4 keV linked to the 1^+ 491.0 keV level by the 170.3 keV $M1$ transition has spin $I^\pi = 0^+$, 1^+ or 2^+. The 228.4 keV level has then spin $I^\pi = 0^-$, 1^-, 2^- or 3^- because of the 92.0 keV $E1$ transition. Considering the cascade 81.9 ($E1$), 146.5 ($M1$) keV, the difference in spin between the 228.4 keV level and the ground state is $\Delta I \leq 2$. Therefore, the only possibility is to have $I^\pi(228.4\,\mathrm{keV}) = 3^-$, which determines $I^\pi = 2^+$ for the 320.4 keV level. From these determinations one may assign $I^\pi = 2^-$ for the level at 254.3 keV and $I^\pi = 4^+$ for the level at 146.5 keV. For several states, it is difficult to give a unique assignment. It is even the case for the 71.9 keV state $I^\pi = 2^+$ or 3^+ which is fed mainly by the 156.5 keV $E1$ transition de-exciting the 3^- state at 228.4 keV and by five other transitions.

4 Discussion

In the following discussion we shall attempt to gain a qualitative understanding of the level scheme obtained for ^{184}Au.

4.1 Zero-order level scheme

The study of the neighboring odd-A nuclei of ^{184}Au allows the identification of the single-particle states present at low energy and suggests the neutron-proton configuration which may be observed at low energy.

The nuclei ^{185}Au and ^{183}Au have both a ground state in the $\pi h_{9/2}$ configuration. For the ^{183}Pt and ^{185}Hg nuclei, the prolate deformed states present at low energy are $1/2^-[521]$, $7/2^-[514]$ and $9/2^+[624]$, whereas two states with smaller deformation are present in ^{185}Hg belonging to the $p_{3/2}$ and $i_{13/2}$ shells.

A zero-order approximation of the spectrum of ^{184}Au can be obtained by coupling the proton states present in ^{185}Au and ^{183}Au to the neutron states observed in ^{183}Pt and ^{185}Hg, refs. [29–32], through the procedure described in ref. [33]. This kind of approximation gives a qualitative idea of the relative energy location of the different configurations. We can see in fig. 9 the states that are expected at very low energy.

4.2 Identification of configurations

The identification of the 2^+ isomeric and 5^+ ground states as the $\nu 1/2^-[521] \otimes \pi h_{9/2}$ and $\nu 7/2^-[514] \otimes \pi h_{9/2}$ states, respectively [3,4], has been confirmed by laser spectroscopy. The mean square charge radius changes added to the quadrupole moment values have shown that these two states correspond to a deformed nucleus with $\beta = 0.25$ and that only the orbital $\pi 3/2^-[532]$ arising from the $\pi h_{9/2}$ subshell seems to be involved in the configuration [5]. This means that the 5^+ ground state unambiguously corresponds to the $\nu 7/2^-[514] \otimes \pi 3/2^-[532]$ configuration and the 2^+ isomeric state to the $\nu 1/2^-[521] \otimes \pi 3/2^-[532]$ one. The 5^+ and 2^+ states are then the favored states of these configurations according to the spin parallel coupling rule formulated by Gallagher and Moskowski [34].

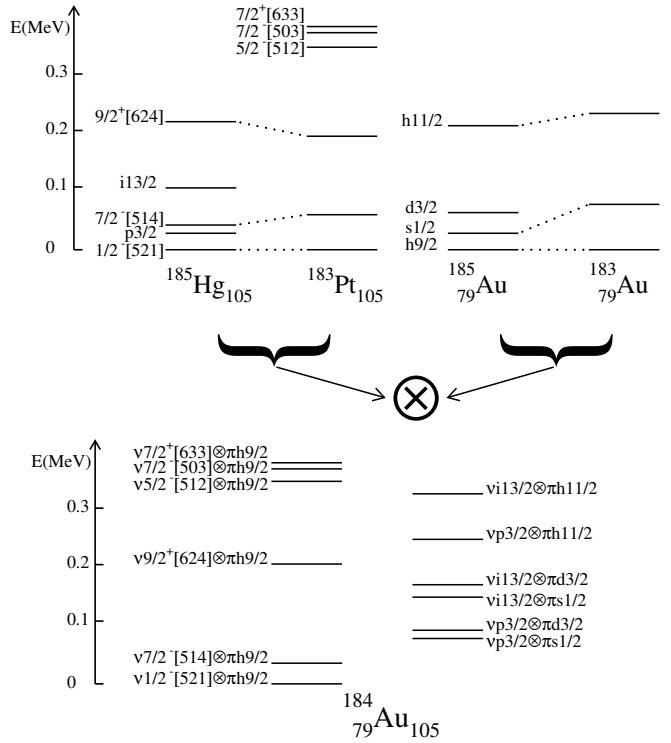

Fig. 9. The neutron and proton states observed at low energy in ^{185}Hg,^{183}Pt and ^{185,183}Au are shown at the top. The zero-order level scheme of ^{184}Au obtained by the coupling of these neutron and proton states is drawn at the bottom.

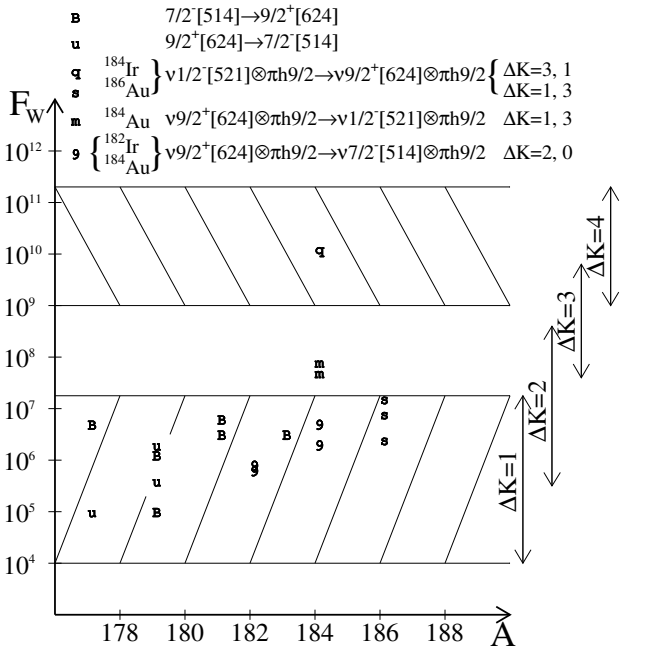

Fig. 10. Comparison of the hindrance factors determined for the $E1$ transitions of the doubly odd ^{184}Au nucleus with those known for similar transitions in the neighboring doubly odd and odd-neutron nuclei.

The negative-parity rotational band observed in the in-beam experiment has a $\nu 9/2^+[624] \otimes \pi h_{9/2}$ configuration. Since the $\pi 3/2^-[532]$ orbital coming from the $\pi h_{9/2}$ subshell seems to be the orbital involved in ^{184}Au, the bandhead of the $\nu 9/2^+[624] \otimes \pi h_{9/2}$ configuration is expected to be a 3^- state from the Gallagher and Moskowski coupling rule [34]. This strongly suggests that the 3^- level located at 228.4 keV has the $\nu 9/2^+[624] \otimes \pi h_{9/2}$ configuration. This enables us to compare the hindrance factors calculated in ^{184}Au with those obtained in the odd nuclei for the corresponding neutron transitions.

In fig. 10 we present the hindrance factors obtained for the transitions de-exciting the 228.4 keV level. We have also displayed the factors calculated for transitions between different states in neighboring nuclei:

– between the $7/2^-[514]$ and the $9/2^+[624]$ states for the odd-N nuclei;

– and for the $\nu 1/2^-[521] \otimes \pi h_{9/2} \rightarrow \nu 9/2^+[624] \otimes \pi h_{9/2}$ and $\nu 9/2^+[624] \otimes \pi h_{9/2} \rightarrow \nu 7/2^-[514] \otimes \pi h_{9/2}$ transitions in the odd-odd nuclei ^{184,182}Ir and ^{186}Au [35, 36].

The isomeric level at 228.4 keV with $I^\pi = 3^-$ decays to the 146.5 and 71.9 keV levels via two $E1$ transitions with hindrance factors $F_W = 4.3 \cdot 10^6$ and $F_W = 1.8 \cdot 10^6$, respectively. These transitions are very similar to those observed in ^{181}Os and ^{183}Pt corresponding to the transition between the neutron states $9/2^+[624]$ and $7/2^-[514]$. The hindrance factors for these two transitions in ^{181}Os and ^{183}Pt are $F_W = 2.5 \cdot 10^6$ and $F_W = 5.6 \cdot 10^6$, respectively. We have therefore a qualitative information that the levels observed in ^{184}Au at 71.9 and 146.5 keV could have the same configuration as the ground state, namely $\nu 7/2^-[514] \otimes \pi h_{9/2}$. In particular, the 71.9 keV level could be the 2^+ partner (spin antiparallel coupled state) of the ground state.

The 160.0 keV and 141.8 keV transitions in ^{184}Au have very similar hindrance factors $F_W = 8.4 \cdot 10^7$ and $F_W = 4.7 \cdot 10^7$, respectively. Furthermore, they are more delayed than the other two transitions decaying the 228.4 keV level by more than an order of magnitude. This suggests that the 86.6 keV level could have the same configuration as the 68.5 keV isomeric state, namely $\nu 1/2^-[521] \otimes \pi h_{9/2}$. Besides, the F_W values of these transitions are between those obtained for the $\nu 1/2^-[521] \otimes \pi h_{9/2} \rightarrow \nu 9/2^+[624] \otimes \pi h_{9/2}$ transition in ^{184}Ir and ^{186}Au (see fig. 10), which seems rather consistent with the proposed configurations.

On the other hand, if the 2^- state has the $\nu p_{3/2} \otimes \pi s_{1/2}$ configuration (see fig. 9), it would be impossible to explain the favored $M1$ link between the 2^- and the 3^- levels since this transition would imply a Δl forbidden transition for both the neutron and the proton.

To go further in the understanding of the structure of the low-lying states in ^{184}Au we shall now use theoretical predictions.

4.3 Theoretical calculations

The theoretical calculations were performed using the semi-microscopic model developed by Bennour *et al.* [7]. In this approach two quasiparticles are coupled to an axial rotor with a variable moment of inertia that is deduced from the experimental energy sequence observed in the even-even core.

To determine the equilibrium deformation and other static properties of the core, HF + BCS calculations [37–39] were first carried out using the Skyrme III force [40] and usual pairing interaction with constant matrix elements ($G_{\rm op}$ and $G_{\rm on}$) and standard cutoff. The quasiparticle wave functions and the occupation probabilities v^2 of the proton and neutron states of the core also provided by these calculations are used to perform the two-quasiparticle–rotor coupling. In this latter treatment, the proton-neutron interaction, $V_{\rm pn}$, used is the Skyrme III force, *i.e.* the same force as that used to determine the wave functions, v^2 values and static properties of the core, which ensures consistency. On the other hand, the particle number being not conserved in this approach, the four neighboring cores can be used to predict the coupled states which should be involved in the doubly odd nucleus.

Therefore, we performed the HF + BCS calculations for the ^{182,184}Pt cores using $G_{\rm op} = 13.5$, $G_{\rm on} = 15.2$ MeV and for the ^{184,186}Hg cores using $G_{\rm op} = 13.4$, $G_{\rm on} = 14.9$ MeV. Thus, the following equilibrium deformation parameters β were determined:

$\beta = 0.293$ for the ^{182}Pt core,
$\beta = 0.266$ for the ^{184}Pt,
$\beta = 0.280$ for the ^{184}Hg,
$\beta = 0.267$ for the ^{186}Hg.

These β values are larger than that, $\beta = 0.25$, experimentally determined for ^{184}Au [5]. Furthermore, laser spectroscopy measurements have shown that the coupling of one or two quasiparticles to a core may easily change the nuclear deformation in this region [41–47].

All these facts led us to carry out HFC + BCS calculations constraining the core to have two weaker deformations, namely $\beta = 0.25$ and $\beta = 0.22$. The twelve sets of wave functions and v^2 values obtained allowed us to study the influence of a nuclear-deformation change on the relative energy location of the coupled states in the ^{184}Au nucleus. We have to notice that the coupled states calculated for each core can belong to any of the four neighboring doubly odd nuclei. However, the v^2 values that are directly related to the state position under or above the Fermi level may help us to choose the core that should be used to obtain the best description of a given configuration in the doubly odd ^{184}Au nucleus. If an orbital of the core is occupied, v^2 close to 1, it is then only possible to remove a nucleon from it leading rather to the description of the $A-1$ nucleus. Thus, if both the neutron and proton orbitals are occupied we get rather the description of the $A-2$ nucleus. On the other hand, if the neutron and proton orbitals are empty, v^2 close to 0, nucleons can be added and we get rather the description of the $A+2$ nucleus. The v^2 values of the neutron and proton states obtained in the calculations performed for the four cores with a $\beta = 0.25$ deformation are reported in table 5.

Table 5. Occupation probabilities obtained for neutron and proton states of the core.

State	$^{182}_{78}$Pt$_{104}$	$^{184}_{78}$Pt$_{106}$	$^{184}_{80}$Hg$_{104}$	$^{186}_{80}$Hg$_{106}$
$\nu 1/2^-[521]$	0.83	0.96	0.84	0.97
$\nu 7/2^-[514]$	0.76	0.95	0.76	0.95
$\nu 9/2^+[624]$	0.12	0.24	0.12	0.24
$\nu 7/2^+[633]$	0.78	0.95	0.85	0.97
$\pi 3/2^-[532]$	0.20	0.24	0.56	0.60
$\pi 1/2^-[541]$	0.72	0.64	0.88	0.86

Furthermore, calculations have been performed with or without the $V_{\rm pn}$ interaction to point out its influence on the state energies.

The moments of inertia used for Pt cores have been calculated from experimental state energies of the ground-state band without any change for the three deformations. In the case of the Hg cores, the situation is a bit more complicated since the ^{184,186}Hg ground-state bands correspond to quasispherical nuclei. In both cases the deformed band is located at rather low energy above the ground-state and the energy locations of its first states are expected to be perturbed. Therefore, to calculate the moment of inertia of the Hg cores, for states with $I^\pi \geq 10^+$ the experimental energies have been used. For states with $I^\pi = 8^+$, 6^+ and 4^+ the energies have been determined by linear extrapolations. The energy of the 2^+ states have been obtained by comparison with the isotone Pt cores.

4.3.1 Positive-parity states

It is clear that the positive-parity states corresponding to the $\nu 1/2^-[521] \otimes \pi 3/2^-[532]$ and $\nu 7/2^-[514] \otimes \pi 3/2^-[532]$ configurations should be reproduced better by calculations performed using either the ^{184}Pt core or the ^{186}Hg core because of the v^2 values close to 1 for the involved neutron states. Besides, the laser spectroscopy results indicate that the coupled proton of the isomeric and ground states of ^{184}Au mainly occupies the $3/2^-[532]$ state. This fact is well reproduced for calculations with the ^{186}Hg but not for calculations with the ^{184}Pt core for which the favored state corresponds to the coupled proton in the $1/2^-[541]$ state. Therefore, later on for the positive-parity states we shall show the comparison of the experimental results only with the predictions obtained with the ^{186}Hg core.

Firstly, to illustrate the influence of the core deformation on the relative energy of the first levels of the $\nu 7/2^-[514] \otimes \pi h_{9/2}$ and $\nu 1/2^-[521] \otimes \pi h_{9/2}$ configurations that one believes the most probable structure of the ground and isomeric states of ^{184}Au, we have reported in fig. 11 for three different β deformations of the ^{186}Hg core:

– the 6^+, 5^+ and 4^+ states predicted with $V_{\rm pn}$ for the ground-state configuration,

Table 6. Main components (in %) of the wave functions calculated with the $V_{\rm pn}$ interaction using a ^{186}Hg core with $\beta = 0.25$ deformation. The experimental energies (fig. 8 or [48]) of the levels for which an identification is proposed, are given in the last column; in case of two possible identifications the energies are given in parenthesis and reported twice.

I^π	E	$\nu 7/2^-[514] \otimes \pi 3/2^-[532]$		$\nu 7/2^-[514] \otimes \pi 1/2^-[541]$		$\nu 1/2^-[521] \otimes \pi 3/2^-[532]$		$E_{\rm exp}$
	(keV)	$K=5$	$K=2$	$K=4$	$K=3$	$K=2$	$K=1$	(keV)
6^+	-20	58	–	20	17	–	–	83.6
5^+	0	47	6	31	15	–	–	0
4^+	54	–	34	27	39	–	–	146.5
3^+	69	–	38	–	16	26	–	(71.9)
7^+	70	49	–	32	14	–	–	187
2^+	85	–	80	–	–	–	10	(71.9)
8^+	185	43	6	34	17	–	–	311
9^+	328	38	7	35	19	–	–	457
10^+	497	35	7	36	21	–	–	624
I^π	E	$\nu 1/2^-[521] \otimes \pi 3/2^-[532]$		$\nu 1/2^-[521] \otimes \pi 1/2^-[541]$		$\nu 7/2^-[514] \otimes \pi 3/2^-[532]$		$E_{\rm exp}$
	(keV)	$K=2$	$K=1$	$K=1$	$K=0$	$K=5$	$K=2$	(keV)
2^+	61	40	17	20	8	–	15	68.5
3^+	80	29	–	16	9	–	30	–
4^+	109	28	21	32	18	–	–	–
5^+	120	32	7	27	24	–	–	–
1^+	138	–	77	22	–	–	–	(129.2)
2^+	142	51	34	–	9	–	–	(129.2)
3^+	226	9	68	–	20	–	–	–
4^+	254	49	35	–	11	–	–	–
1^+	257	–	5	36	59	–	–	306.9
6^+	263	24	18	33	21	–	–	–
7^+	277	27	10	33	29	–	–	–
0^+	380	–	–	–	99.8	–	–	–
1^+	502	–	17	42	40	–	–	–
9^+	530	23	11	34	31	–	–	–
11^+	862	21	11	34	32	–	–	–
I^π	E	$\nu 9/2^+[624] \otimes \pi 3/2^-[532]$		$\nu 9/2^+[624] \otimes \pi 1/2^-[541]$		$\nu 7/2^+[633] \otimes \pi 3/2^-[532]$		$E_{\rm exp}$
	(keV)	$K=3$	$K=6$	$K=4$	$K=5$	$K=2$	$K=5$	(keV)
3^-	−310	94	–	–	–	–	–	228.4
6^-	−267	–	87	–	9	–	–	–
4^-	−256	84	–	10	–	–	–	–
5^-	−199	72	–	19	–	–	–	–
7^-	−188	–	69	5	17	–	–	–
8^-	−104	5	54	9	22	–	–	-
9^-	0	6	44	12	24	–	–	–
5^-	35	11	–	10	62	–	13	–
4^-	116	8	–	76	–	–	–	–
I^π	E	$\nu 7/2^+[633] \otimes \pi 3/2^-[532]$		$\nu 7/2^+[633] \otimes \pi 1/2^-[541]$		$\nu 9/2^+[624] \otimes \pi 1/2^-[541]$		$E_{\rm exp}$
	(keV)	$K=2$	$K=5$	$K=3$	$K=4$	$K=4$	$K=5$	(keV)
5^-	297	10	39	26	15	9	–	
2^-	326	99	–	–	–	–	–	254.3
3^-	329	67	–	24	–	–	–	–
4^-	334	47	–	36	16	–	–	–
6^-	352	11	33	24	29	–	–	–
7^-	445	11	30	23	29	–	–	–

– the 2^+ and 3^+ states calculated with $V_{\rm pn}$ for the isomeric state configuration.

To compare experimental and theoretical results, the 2^+ isomeric and 5^+ ground states of ^{184}Au as well as the state having 4^+ as unique spin value and the same particle configuration as the ground state have also been reported in fig. 11. It appears clearly that the relative energy of the isomeric and ground states of ^{184}Au is best reproduced for $\beta = 0.25$, which is in agreement with the laser spectroscopy data [5]. The 6^+ state predicted at 20 keV below the 5^+ one for $\beta = 0.25$, has not been observed in ^{184}Au but such a state probably located at very low energy above the ground state is not fed in the Hg radioactive decay because the nearby 5^+ state collects the transitions.

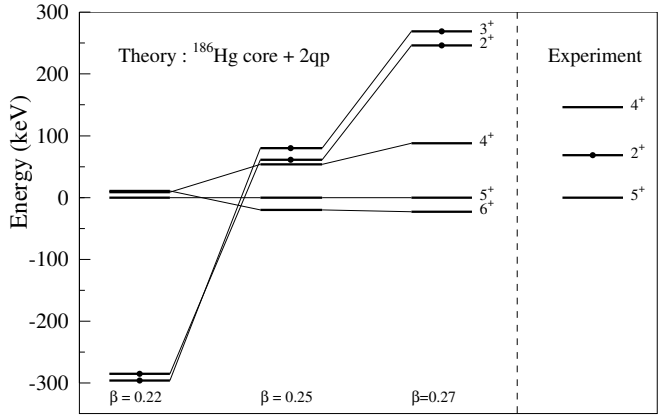

Fig. 11. Comparison of the relative energy position of the 2^+ isomeric and 5^+ ground states of ^{184}Au with the energy evolution of the first states of the $\nu 1/2^-[521] \otimes \pi h_{9/2}$ and $\nu 7/2^-[514] \otimes \pi h_{9/2}$ configurations calculated using the ^{186}Hg core with three different deformations: $\beta = 0.22$, 0.25 and 0.27. The 5^+ states have been placed at an energy equal to zero arbitrarily.

It is worth noting that the 2^+, 3^+ and 6^+, 5^+ state inversions are related to a change of the main component of the coupled proton from the $\pi 3/2^-[532]$ state for $\beta = 0.25$ and $\beta = 0.27$ to the $\pi 1/2^-[541]$ state for $\beta = 0.22$.

Moreover, for the ground-state configuration at $\beta = 0.25$ the favored coupling is $\nu 7/2^-[514] \otimes \pi 3/2^-[532]$ with $K = 5$; it is rather surprising that the 6^+ state is predicted to be located at the lowest energy. This is likely due to the weaker component $\nu 7/2^-[514] \otimes \pi 3/2^-[532]$ $K = 5$ in the wave function of the 5^+ than in that of the 6^+ state, which increases the energy of the 5^+ level relatively to the 6^+ one (see table 6).

Secondly, to perform a more complete comparison of the experimental and theoretical results we have reported in fig. 12 the experimental levels identified as belonging to the ground- and isomeric-state configurations either in the present work for levels with $I \leq 5$ or in in-beam spectroscopy measurements for levels with $I \geq 5$ in refs. [4,48], together with predicted states of both the $\nu 7/2^-[514] \otimes \pi h_{9/2}$ and $\nu 1/2^-[521] \otimes \pi h_{9/2}$ configurations calculated using a ^{186}Hg core with a $\beta = 0.25$ deformation and taking into account, or not, the $V_{\rm pn}$ interaction. In this figure are also shown the states of the core deduced from experimental results that have been used to calculate the variable moment of inertia of the deformed ^{186}Hg nucleus. We can see in fig. 12 that the $V_{\rm pn}$ interaction changes mainly the energy location of low-spin states. For example, in the case of the ground-state configuration, the 2^+ and the 3^+ states calculated at the lowest energies without $V_{\rm pn}$ are about 100 keV above the 6^+ and the 5^+ states when the $V_{\rm pn}$ interaction is taken into account.

We have to note that for the ground-state configuration one of the two states with $I \leq 3$ predicted with excitation energies smaller than 100 keV has not been observed in the present work. On the other hand, for the isomeric configuration three low-spin states are predicted at low energy: a 1^+ state at 138 keV, a 2^+ state at 142 keV and a 1^+ state at 257 keV. One of the two first states could correspond to the level with $I^\pi = 1$, 2^+ established at 129.2 keV and the third one to the 1^+ level established at 306.9 keV in ^{184}Au (see fig. 8). These two levels have been reported in dotted lines in fig. 12.

The main components of the wave function of some of the states shown in fig. 12 are listed in table 6. One can see a very important admixture in all the wave functions, the coupled proton occupying either the $3/2^-[532]$ or the $1/2^-[541]$ state. Moreover, for the yrast states, there is a gradual change of the main component when I increases: i) for the $\nu 7/2^-[514] \otimes \pi h_{9/2}$ configuration, the proton is mainly in the $3/2^-[532]$ state for $I \leq 7$, whereas the proton comes mainly into the $1/2^-[541]$ state for $I > 7$, ii) for the $\nu 1/2^-[521] \otimes \pi h_{9/2}$ configuration, the same change of the proton state takes place around $I = 4$. Band crossings at low energy are responsible for these structure changes of the yrast states. The very important admixtures calculated for the 2^+ isomeric and the 5^+ ground states disagree with the rather pure $K = 2$ and $K = 5$ values deduced from the spectroscopic quadrupole moments measured: $Q_S = 1.90(16)$ b for the 2^+ state and $Q_S = 4.65(26)$ b for the 5^+ state [4]. The calculated admixtures reported in table 6 lead to $Q_S = 0.62$ b and $Q_S = 2.45$ b for the 2^+ and 5^+ states, respectively. It is worth noting that calculations performed using the other cores also overestimate the K admixtures. The comparison of the predicted Q_S values with the experimental results has already been discussed in ref. [49].

The ^{184}Hg nucleus in its 0^+ ground state has a quasi-spherical shape. Its β decay towards the 491.0 keV level in ^{184}Au is the most favored. We can guess that it corresponds to a β transition between spin-orbit partners. The proton subshells available under the magic number $Z = 82$ are $s_{1/2}$, $d_{3/2}$, $h_{11/2}$, $d_{5/2}$ and $g_{7/2}$ and the neutron ones around $N = 100$ are $i_{13/2}$ and $h_{9/2}$. Therefore, the favored β transition could correspond to a change of a proton $h_{11/2}$, to a neutron $h_{9/2}$ leading to a $\nu h_{9/2} \otimes \pi h_{11/2}$ configuration for the 1^+ state located at 491 keV. It is impossible to know if this 1^+ state keeps or not the quasi-spherical shape of ^{184}Hg. Anyway, it is probable that it is not one of the three 1^+ states of the $\nu 1/2^-[521] \otimes \pi h_{11/2}$ configuration since it decays mainly towards the 2^- state at 254.3 keV. However, the shape of the neighboring ^{186}Au nucleus in its strongly fed 1^+ state has already been discussed and by comparison with the data known for the heavier gold isotopes, it was concluded that the 1^+ state seems to correspond to a quasispherical shape [36].

4.3.2 Negative-parity states

The de-excitation mode of the short-lived 3^- isomeric state established in the present work and the properties of the negative-parity rotational band observed in the in-beam experiment [4] strongly suggest that the low-lying negative-parity states of ^{184}Au could correspond to the $\nu 9/2^+[624] \otimes \pi 3/2^-[532]$ configuration. Besides, the 3^- state should be the bandhead of a configuration as it is

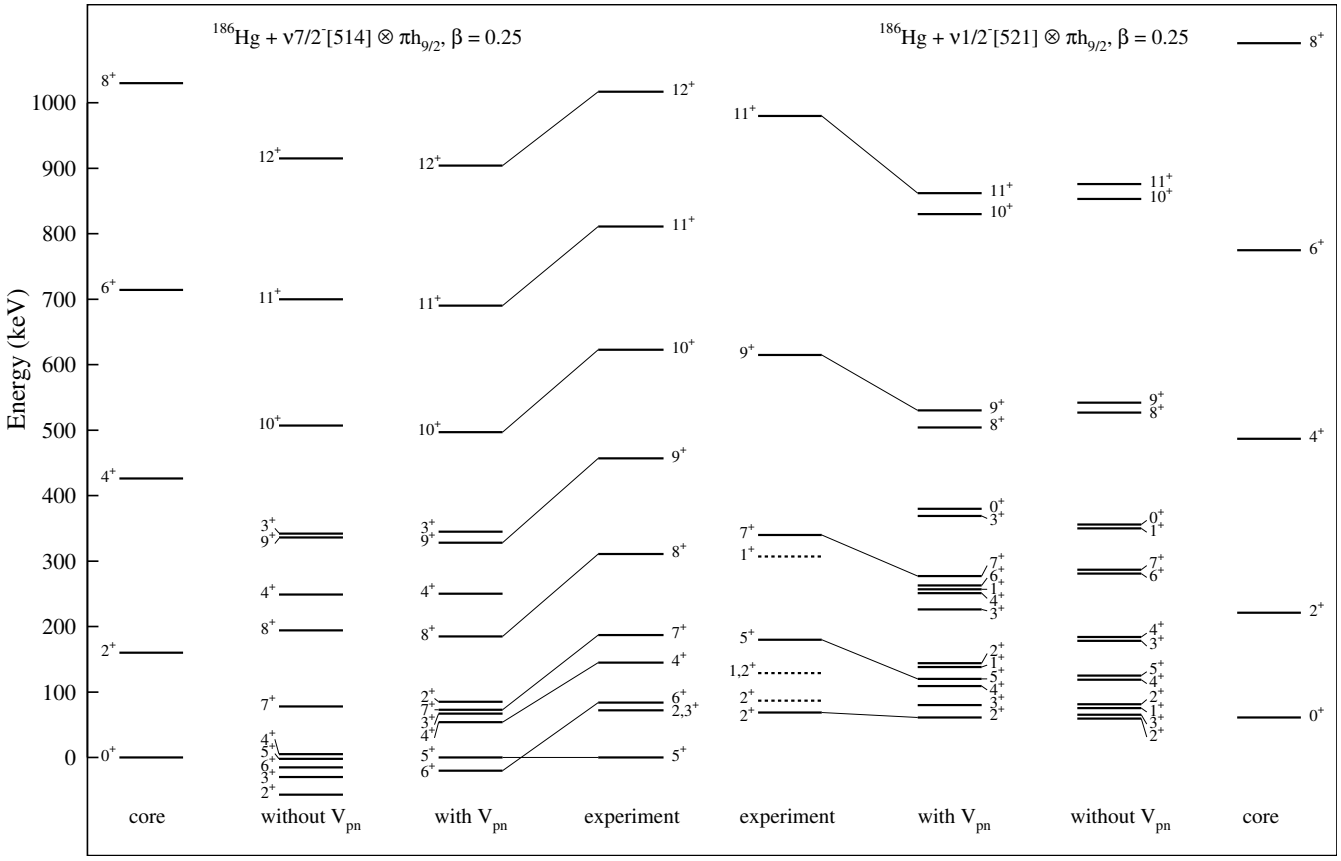

Fig. 12. Comparison of the observed positive-parity states to the predicted ones for the $\nu 7/2^-[514] \otimes \pi h_{9/2}$ and $\nu 1/2^-[521] \otimes \pi h_{9/2}$ configurations obtained using the ^{186}Hg core at a $\beta = 0.25$ deformation. For the predicted states with $4 < I \leq 11$ only the yrast states are reported, whereas for those with $I < 5$ and located under 400 keV all the states are shown.

the negative-parity state located at the lowest energy. The nuclear deformation of these negative-parity states has not been measured. In Pt isotopes, the deformation is increased by a single neutron in the $9/2^+[624]$ state or in the $7/2^-[514]$ state, whereas the deformation change is less important for a neutron in the $1/2^-[521]$ state [45]. Nevertheless, the doubly odd ^{184}Au nucleus has almost the same deformation in the $\nu 1/2^-[521] \otimes \pi 3/2^-[532]$ isomeric state as in the $\nu 7/2^-[514] \otimes \pi 3/2^-[532]$ ground state [5]. This fact suggests that the deformation of ^{184}Au in the negative-parity states should be also very close to that of the ground state, $\beta = 0.25$.

From the v^2 values, none of the four cores is, *a priori*, more suitable than the others to reproduce the data of the negative-parity states of ^{184}Au. The states due to the $\nu i_{13/2} \otimes \pi h_{9/2}$ coupling are predicted at rather low energy in the calculations performed with the ^{182,184}Pt and ^{186}Hg cores. They are distributed over four families of states corresponding to the following main configurations:

1. $\nu 9/2^+[624] \otimes \pi 1/2^-[541]$ with $K = 4$ and 5,
2. $\nu 9/2^+[624] \otimes \pi 3/2^-[532]$ with $K = 3$ and 6,
3. $\nu 7/2^+[633] \otimes \pi 1/2^-[541]$ with $K = 3$ and 4,
4. $\nu 7/2^+[633] \otimes \pi 3/2^-[532]$ with $K = 2$ and 5.

The family predicted at the lowest energy for $\beta = 0.25$ corresponds to:

- the first configuration with the ^{184}Pt core;
- the second one with the ^{184}Hg and ^{186}Hg cores; but in the case of ^{184}Hg core, all the states are located at a rather high energy (above 650 keV);
- the third one with the ^{182}Pt core.

We have to note that a 3^- bandhead is found only for the $\nu 9/2^+[624] \otimes \pi 3/2^-[532]$ configuration. Moreover, the first configuration has no 3^- state. All these facts indicate that the ^{186}Hg nucleus with $\beta = 0.25$, is the best core to reproduce the properties of the 3^- bandhead of the negative-parity states. Therefore, in fig. 13 we compare the experimental results to the predictions obtained with the ^{186}Hg core at $\beta = 0.25$ and taking into account, or not, the $V_{\rm pn}$ interaction. We can see that the $V_{\rm pn}$ interaction modifies slightly the energy location of the low-spin states as for the positive-parity states.

The 2^- state with a pure $\nu 7/2^+[633] \otimes \pi 3/2^-[532]$ configuration, even though it is predicted with $V_{\rm pn}$ at 630 keV above the 3^- state could correspond to the 2^- level observed at only 26 keV above the 3^-. Thus, the favored $2^- \rightarrow 3^-$ link could be understood since it would correspond to the favored $\nu 7/2^+[633] \otimes \pi 3/2^-[532] \rightarrow$

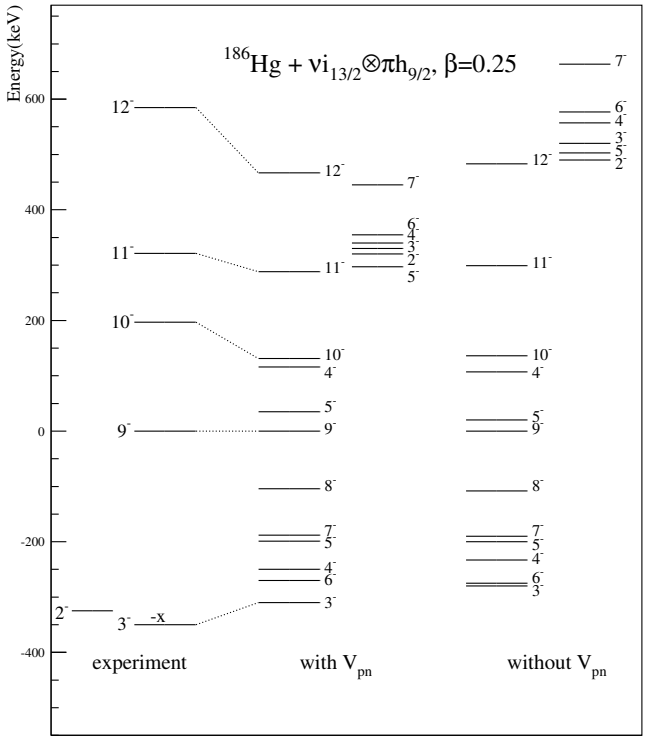

Fig. 13. Comparison of the negative-parity states of ^{184}Au observed in the present work and in the in-beam experiment [4] to those of the $\nu i_{13/2} \otimes \pi h_{9/2}$ coupling calculated using a ^{186}Hg core at $\beta = 0.25$. For the predicted states with $I > 6$ only the yrast states are reported, whereas all the states with $I < 6$ and located at an energy lower than 650 keV are shown. The two 9^- states have been located at 0 arbitrarily.

$\nu 9/2^+[624] \otimes \pi 3/2^-[532]$ transition. It is worth noting that none of the other 2^- calculated states could have such a favored link towards the 3^- state.

We can see in fig. 13 that the sequence of the calculated states for the $\nu 9/2^+[624] \otimes \pi h_{9/2}$ configuration is much more regular than the experimental one. The main components of the wave functions of most of the states displayed in fig. 13 are listed in table 6. No large admixtures of the two configurations are predicted in the wave functions of these states, due to the large energy spacing calculated between the $\nu 9/2^+[624] \otimes \pi h_{9/2}$ and $\nu 7/2^+[633] \otimes \pi h_{9/2}$ configurations. Indeed, if the states of these configurations were calculated at close energies, according to the experimental location, then components of the $\nu 7/2^+[633] \otimes \pi h_{9/2}$ configuration would appear in the wave function of the states of the $\nu 9/2^+[624] \otimes \pi h_{9/2}$ main configuration and perturb the calculated sequence.

The energy distance of the $\nu 9/2^+[624]$ and $\nu 7/2^+[633]$ states is also calculated too large for the odd-A nuclei: it is calculated equal to 550 keV with the ^{184}Pt and ^{186}Hg cores, whereas it is only 179 keV in ^{183}Pt. This anomaly is due, in part, to the position of the Fermi level that is not exactly the one of the odd-A or doubly odd nucleus but that of the core.

Moreover, in ^{186}Au, such a 2^- level with probable $\nu 7/2^+[633] \otimes \pi h_{9/2}$ configuration exists and it is located at only 36 keV above the 3^- ground state with the $\nu 9/2^+[624] \otimes \pi h_{9/2}$ configuration [36]. In ^{182}Au, the first negative-parity state located at 129 keV [50], and that has probable spin and parity values $I^\pi = 2^-$, could also have a $\nu 7/2^+[633] \otimes \pi h_{9/2}$ main configuration, the $I^\pi = 3^-$ level with the $\nu 9/2^+[624] \otimes \pi h_{9/2}$ configuration is then very likely located above the 2^- level, which explains why it was not observed in the β decay of ^{182}Hg [50]. Thus, the relative energy evolution of the 3^- and 2^- levels of the doubly odd Au nuclei from $A = 186$ to $A = 182$ would be in qualitative agreement with the decrease of the energy distance of the $\nu 7/2^+[633]$ and $\nu 9/2^+[624]$ states in the odd-A Pt nuclei that is 706 keV for $A = 185$, 179 keV for $A = 183$ and 11 keV for $A = 181$, refs. [31,51,52].

5 Conclusion

Three series of experiments have been performed to study the β^+/EC decay of ^{184}Hg. Coincidences and conversion electrons precisely measured allowed us to build a level scheme of ^{184}Au: 16 excited levels have been clearly established and for 10 of them unique spin and parity values have been determined. Experimental properties: energies, spin and parity values, sequence in rotational band [4], deformation, nuclear moments [5] and de-excitation modes, suggested the nuclear structure of some levels of ^{184}Au, namely: $\nu 7/2^-[514] \otimes \pi 3/2^-[532]$ for the ground state, $\nu 1/2^-[521] \otimes \pi 3/2^-[532]$ for the 2^+ isomeric state at 68.5 keV and $\nu 9/2^+[624] \otimes \pi 3/2^-[532]$ for the 3^- short-lived isomeric state at 228.4 keV.

A comparison of the experimental levels with the states calculated by use of the semi-microscopic axial-rotor–plus–two-quasiparticle model [7] allows us to confirm the three suggested configurations above mentioned and to identify some other low-spin levels:

- the 2, 3^+ level located at 71.9 keV and the 4^+ one at 146.5 keV have the same $\nu 7/2^-[514] \otimes \pi h_{9/2}$ configuration as the 5^+ ground state;
- the 2^+ level located at 86.6 keV, the 1, 2^+ state at 129.2 keV and the 1^+ level at 306.9 keV could have the same $\nu 1/2^-[521] \otimes \pi h_{9/2}$ configuration as the 2^+ isomeric state;
- the 2^- level located at 254.3 keV, very likely, corresponds to the $\nu 7/2^+[633] \otimes \pi h_{9/2}$ configuration.

In spite of the rather good agreement obtained for the energy spectra of the positive-parity states, the admixtures in the wave functions are found very much at variance with the quadrupole moment results that indicate that the proton occupies the $3/2^-[532]$ orbital and not the $1/2^-[541]$ one. Thus, the model calculates too strong admixtures due to an overestimation of the Coriolis effect. On the other hand, the calculations certainly underestimate the admixtures in the wave functions of the negative-parity states because of the too large energy spacing calculated between the $\nu 9/2^+[624]$ and $\nu 7/2^+[633]$

quasineutron states due to the Fermi level location. Finally, for the negative-parity states we should like to emphasize that it would be very interesting to get the link between the 9^- state and the 3^- bandhead to support the $\nu 9/2^+[624] \otimes \pi h_{9/2}$ configuration attributed therein to the 9^- state.

References

1. J.L. Wood *et al.*, Phys. Rep. **215**, 101 (1992); K. Heyde *et al.*, Phys. Rep. **102**, 291 (1983).
2. R. Eder *et al.*, *Proceedings of the Eighth International Conference on Hyperfine Interactions*, Hyperfine Interact. **60**, 83 (1990).
3. F. Ibrahim *et al.*, Z. Phys. A **350**, 9 (1994).
4. F. Ibrahim *et al.*, Phys. Rev. C **53**, 1547 (1996).
5. F. Le Blanc *et al.*, Phys. Rev. Lett. **79**, 2213 (1997).
6. C.M. Baglin in `http://www.nndc.gov/userout/AR_42464_2.html`
7. L. Bennour, J. Libert, M. Meyer, P. Quentin, Nucl. Phys. A **465**, 35 (1987).
8. A. Ben Braham *et al.*, Nucl. Phys. A **332**, 397 (1979).
9. C. Sebille-Schück *et al.*, Nucl. Phys. A **212**, 45 (1973).
10. P. Kilcher *et al.*, Nucl. Instrum. Methods A **274**, 485 (1989).
11. B. Roussière *et al.*, Nucl. Phys. A **643**, 331 (1998).
12. B. Roussière *et al.*, Hyperfine Interact. **129**, 119 (2000).
13. A. Plantier *et al.*, Nucl. Instrum. Methods B **26**, 314 (1987).
14. C. Deprun, Orsay report IPNO-RC-75-02.
15. R. Gunnink, J.B. Niday, *Computerized Quantitative Analysis by γ-ray Spectroscopy*, Lawrence Livermore Laboratory, Report No. UCRL-51061, Vol. **1** (1972).
16. H. Dautet, private communication.
17. S.E.T.I., Rapport interne IPNO 87-03.
18. R.S. Hager, E.C. Seltzer, Nucl. Data A **4**, 1 (1968).
19. F. Rösel, H.H. Fries, K. Alder, A.C. Pauli, At. Data Nucl. Data Tables **21**, 91 (1978).
20. B. Roussière *et al.*, Nucl. Phys. A **548**, 227 (1992).
21. M. de Jésus, Thèse, Université Lyon (1992).
22. J.L. Wood *et al.*, Phys. Rev. C **55**, 2697 (1997).
23. E.L. Church, J. Weneser, Annu. Rev. Nucl. Phys. **10**, 193 (1960).
24. R.J. Lombard, Phys. Lett. **9**, 254 (1964).
25. W.G. Nettles *et al.*, J. Phys. **39**, 343 (1978).
26. H. Dautet *et al.*, *Proceedings of the 7th International Conference on Atomic Masses and Fundamental Constants, AMCO7* (1984) p. 257.
27. G. Audi, A.H. Wapstra, C. Thibault, Nucl. Phys. A **729**, 337 (2003).
28. S. Raman, B. Gove, Phys. Rev. C **7**, 1995 (1973).
29. C. Bourgeois *et al.*, Nucl. Phys. A **386**, 308 (1982).
30. M.I. Macias-Marqués *et al.*, Nucl. Phys. A **427**, 205 (1984).
31. B. Roussière *et al.*, Nucl. Phys. A **504**, 511 (1989).
32. P. Kilcher *et al.*, *Proceedings of the 5th International Conference on Nuclei Far from Stability, Rosseau Lake, Ontario, Canada*, AIP Conf. Proc. **164**, 513 (1988).
33. A.J. Kreiner *et al.*, Nucl. Phys. A **432**, 451 (1985).
34. C.J. Gallagher, S.A. Moskowski, Phys. Rev. **111**, 1282 (1958)
35. A. Ben Braham *et al.*, Nucl. Phys. A **482**, 553 (1988).
36. M.G. Porquet *et al.*, Nucl. Phys. A **411**, 65 (1983).
37. D. Vautherin, D.M. Brink, Phys. Rev. C **5**, 626 (1972).
38. D. Vautherin, Phys. Rev. C **7**, 296 (1973).
39. H. Flocard, P. Quentin, A.K. Kerman, D. Vautherin, Nucl. Phys. A **203**, 433 (1973).
40. M. Beiner, H. Flocard, Nguyen Van Giai, P. Quentin, Nucl. Phys. A **238**, 29 (1975).
41. G. Ulm *et al.*, Z. Phys. A **325**, 247 (1986).
42. W. Wallmeroth *et al.*, Nucl. Phys. A **493**, 224 (1989).
43. G. Savard *et al.*, Nucl. Phys. A **512**, 241 (1990).
44. T. Hilberath *et al.*, Z. Phys. A **342**, 1 (1992).
45. F. Le Blanc *et al.*, Phys. Rev. C **60**, 054310 (1999).
46. J. Sauvage *et al.*, *ENAM98*, AIP Conf. Proc. **455**, 585 (1998).
47. D. Verney *et al.*, *International Conference on Experimental Nuclear Physics in Europe Facing the Next Millenium, Sevilla*, AIP Conf. Proc. **495**, 117 (1999).
48. Y.H. Zhang *et al.*, Phys. Rev. C **70**, 057303 (2004); F. Ibrahim, J. Genevey *et al.*, unpublished results.
49. B. Roussière *et al.*, *International Conference on Nuclear Structure and Related Topics, Dubna June 2000*, Yad. Fiz. **64**, 1123 (2001).
50. F. Ibrahim *et al.*, Eur. Phys. J. A **10**, 139 (2001).
51. B. Roussière *et al.*, Nucl. Phys. A **438**, 93 (1985).
52. J. Sauvage *et al.*, Nucl. Phys. A **540**, 83 (1992).